Scattering of acoustic waves by macroscopically inhomogeneous poroelastic tubes

J.-P. Groby,[a] O. Dazel, and C. Depollier
Laboratoire d'Acoustique de l'Université du Maine, UMR6613 Centre National de la Recherche Scientifique/ Université du Maine, Avenue Olivier Messiaen, F-72085 Le Mans Cedex 9, France

E. Ogam
Laboratoire de Mécanique et d'Acoustique, UPR7051 Centre National de la Recherche Scientifique, 31 Chemin Joseph-Aiguier, F-13402 Marseille Cedex 20, France

L. Kelders
Laboratorium voor Akoestiek en Thermische Fysica, KULeuven, Celestijnenlaan 200D, B-3001 Heverlee, Belgium

(Received 20 September 2011; revised 17 April 2012; accepted 29 April 2012)

Wave propagation in macroscopically inhomogeneous porous materials has received much attention in recent years. For planar configurations, the wave equation, derived from the alternative formulation of Biot's theory of 1962, was reduced and solved recently: first in the case of rigid frame inhomogeneous porous materials and then in the case of inhomogeneous poroelastic materials in the framework of Biot's theory. This paper focuses on the solution of the full wave equation in cylindrical coordinates for poroelastic tubes in which the acoustic and elastic properties of the poroelastic tube vary in the radial direction. The reflection coefficient is obtained numerically using the state vector (or the so-called Stroh) formalism and Peano series. This coefficient can then be used to straightforwardly calculate the scattered field. To validate the method of resolution, results obtained by the present method are compared to those calculated by the classical transfer matrix method in the case of a two-layer poroelastic tube. As an example, a long bone excited in the sagittal plane is considered. Finally, a discussion is given of ultrasonic time domain scattered field for various inhomogeneity profiles, which could lead to the prospect of long bone characterization. [http://dx.doi.org/10.1121/1.4725763]

PACS number(s): 43.80.Ev, 43.20.Gp, 43.20.Fn [KVH] Pages: 477–486

I. INTRODUCTION

Propagation of acoustic waves in macroscopically inhomogeneous porous materials has received much attention in the last few years. It was initially motivated by (i) the design of sound absorbing porous materials with optimal material and geometrical property profiles[1] and (ii) the retrieval of the spatially varying material parameters of porous materials, mainly industrial foams.[2] These, and other inverse problems, are of great importance in connection with the characterization of the mechanical properties of naturally occurring macroscopically inhomogeneous porous materials such as bones or rocks. The wave equation in macroscopically inhomogeneous porous media was derived from the alternative formulation of Biot's theory[3] in De Ryck *et al.*[4] and solved in the case of rigid frame inhomogeneous porous materials via the Wave Splitting method and "transmission" Green's functions approach or via an iterative Born approximation procedure based on the specific Green's function of the configuration.[5] The recovery of several profiles of spatially varying material parameters by means of an optimization approach, was then achieved in Ref. 2 still in the rigid frame approximation. Recently, the full wave equation in macroscopically inhomogeneous poroelastic media was solved in a planar configuration, by use of the state vector formalism together with a Peano series.[6]

The present article focuses on circular cylindrical shaped configurations that can be encountered in sonic crystals or array of circular scatterers,[7] geophysics for the interpretation of borehole logs,[8] composites,[9] or appendicular human bones. An example is proposed on appendicular human bones, but the developed formulation is general and can be adapted in the contexts of geophysics or sonic crystals. Effectively, being saturated by a heavy fluid, appendicular bone application is suitable to clearly emphasis the skeleton effect, which is obviously important in this context.

To solve the full wave equation in macroscopically inhomogeneous poroelastic media in cylindrical coordinates, the state vector formalism together with Peano series are employed. The latter methods have been largely used and developed for surface waves or propagation of acoustic waves in inhomogeneous anisotropic elastic plates[10] or in radially inhomogeneous anisotropic elastic cylinders.[11] In this article, radially inhomogeneous bone-like tubes are considered. Problems encountered with such methods in cases of full radially inhomogeneous circular cylinders related to the intrinsic singularity at the central point are not considered and also avoided.[12]

Bone is a live tissue, which is constantly resorbed and formed during the remodeling process. There exist two forms of bone: cortical (or compact) and cancellous (or

[a]Author to whom correspondence should be addressed. Electronic mail: Jean-Philippe.Groby@univ-lemans.fr

trabecular or spongy). Cortical bone predominates in the appendicular portion and cancellous bone in the axial portion, notably the spine. Cortical bone occupies the exterior portion of the long bones, and is arranged as bundles of osteons packed tightly together to resist bending forces. The porosity of cortical bones varies from 0.1 to 0.5. A three-dimensional cortical bone is usually modeled as an anisotropic (transversally isotropic) elastic material.[13–15] Nevertheless, when excited by an acoustic wave that strikes the long bone perpendicular to its axis, a two-dimensional approximation can be made in the sagittal plane: the cortical bone can be modeled by an isotropic elastic material or a poroelastic material. Cancellous bone is lighter and more porous (porosity from 0.6 up to 0.9) and structured to resist compressive forces. Cancellous bone occupies the inner portion of long bones. By cutting a long bone in transverse manner, one can distinguish, from the center towards the periphery: the marrow within the medullary cavity, the spongy bone, and the cortical bone. Recently, ultrasonic bone characterization[16,17] of spongy bones has received much attention in order to develop comprehensive theoretical models, which will be helpful in solving the inverse problem, i.e., in extracting structural and mechanical properties of the bone from ultrasonic measurements. Bone parameters determined in Ref. 17 will be used in the following. The bone will be modeled as a macroscopically inhomogeneous poroelastic tube of circular cross-section, saturated with water. The macroscopically inhomogeneous poroelastic material is assumed isotropic and the inhomogeneity is radial. The incident wave strikes the tube perpendicularly to the tube axis. The marrow and surrounding flesh are also modeled as water. The marrow viscosity is higher than that of water, but it is often assumed to be the same.[14,15]

First, the constitutive linear stress-strain relations and the momentum conservation law in the absence of body forces are recalled for an inhomogeneous poroelastic material. These equations are then solved for a radially macroscopically inhomogeneous poroelastic tube via the state vector formalism or the so-called Stroh formalism[18] together with Peano series.[19,20] Numerical results obtained with this method are compared to calculations of the classical transfer matrix method for a known two-layer porous tube considered as a single inhomogeneous tube. Finally, simple applications for the diagnosis of osteoporosis are proposed, by comparing the time domain diffracted fields by circular cylindrical tube with various radially inhomogeneity profiles that are either continuous or discontinuous. In particular, the numerical results exhibit some differences in these time domain responses from one configuration to another that could be interpreted and used to characterize bones.

II. EQUATIONS OF MACROSCOPICALLY INHOMOGENEOUS POROUS MATERIALS

As pointed out by several authors,[3,21,22] the generalized formulation of the Biot theory[3] is suitable for modeling sound propagation in macroscopically inhomogeneous porous media and also to account for anisotropic and viscoelastic frames. Recently, another formulation was proposed in Ref. 23 that is also suitable to macroscopically inhomogeneous porous media. This article focuses on the alternative Biot formulation, which is largely employed in acoustics and geophysics.

Rather than dealing directly with the arbitrary field $\bar{s}(\mathbf{x},t)$ [with $\mathbf{x}=(r,\theta)$], we prefer to deal with the $s(\mathbf{x},\omega)$, related to $\bar{s}(\mathbf{x},t)$ by the Fourier transform $\bar{s}(\mathbf{x},t)=\int_{-\infty}^{\infty}s(\mathbf{x},\omega)e^{i\omega t}d\omega$, wherein $\omega=2\pi\nu$ is the angular frequency, with ν the frequency. Henceforth, we drop the ω in $s(\mathbf{x},\omega)$ so that it is written $s(\mathbf{x})$.

The stress-strain relations in an initially stress-free, statistically isotropic poroelastic material take the form

$$\begin{cases}\sigma_{ij}=2\mu\varepsilon_{ij}+(\lambda_c\theta-\alpha M\zeta)\delta_{ij},\\ p=M(\zeta-\alpha\theta),\end{cases} \tag{1}$$

where δ_{ij} denotes the Kronecker symbol. The components of the total stress tensor are σ_{ij}, the fluid pressure in the pores is p, and the components of the strain tensor are $\varepsilon_{ij}=1/2(u_{i,j}+u_{j,i})$, with the solid displacement $\mathbf{u}$, $\theta=u_{i,i}$, and $\zeta=-w_{i,i}$ with the fluid/solid relative displacement $\mathbf{w}=\phi(\mathbf{U}-\mathbf{u})$ ($\mathbf{U}$ being the fluid displacement and ϕ the porosity). The Einstein summation notation is implicit in the expressions of θ and ζ. The material properties are the bulk modulus of the closed porosity system, i.e., in which the pore volume is sealed, $\lambda_c=\lambda_b+\alpha^2M$, the Lamé coefficients of the porous skeleton λ_b and μ, an additional elastic parameter M, and an elastic coupling coefficient α.[24]

These mechanical coefficients are related to the P, Q, and R coefficients more commonly used in acoustics[25,26] through

$$\begin{aligned}&\alpha=\phi(Q+R)/R,\quad M=R/\phi^2,\\ &\lambda_c=P-Q^2/R-2\mu+\alpha^2M.\end{aligned} \tag{2}$$

The expressions of P, Q, and R are[25]

$$\begin{aligned}P&=4\mu/3+\frac{(1-\phi)(1-\phi-K_b/K_s)K_s+\phi K_bK_s/\tilde{K}_f}{1-\phi-K_b/K_s+\phi K_s/\tilde{K}_f},\\ Q&=\frac{(1-\phi-K_b/K_s)\phi K_s}{1-\phi-K_b/K_s+\phi K_s/\tilde{K}_f},\\ R&=\frac{\phi^2K_s}{1-\phi-K_b/K_s+\phi K_s/\tilde{K}_f},\end{aligned} \tag{3}$$

where the bulk modulus of the skeleton is $K_b=E_b/3(1-2\nu_b)$, the bulk modulus of the elastic frame is $K_s=E_s/3(1-2\nu_s)$, the shear modulus of the skeleton is $\mu=E_b/2(1+\nu_b)$, with ν_b and ν_s the Poisson coefficients, respectively, of the skeleton and of the elastic frame, E_b and E_s the Young moduli, respectively, of the skeleton and of the elastic frame, and

$$\tilde{K}_f=\frac{K_f}{\gamma-(\gamma-1)\left(1+i\frac{\omega_c'}{\mathrm{Pr}\omega}G(\mathrm{Pr}\omega)\right)^{-1}}, \tag{4}$$

where K_f and ρ_f are the bulk modulus and density of the saturating fluid, γ is the specific heat ratio, Pr is the Prandtl

number, and $\omega_c' = R_t'\phi/\rho_f\tau_\infty$ with τ_∞ the tortuosity and R_t' the "thermal resistivity." The correction function $G(\mathrm{Pr}\omega)$, introduced in Ref. 27 to account for the thermal losses, is

$$G(\mathrm{Pr}\omega) = \sqrt{1 - \mathrm{i}\eta\rho_f \mathrm{Pr}\omega\left(\frac{2\tau_\infty}{R_t'\phi\Lambda'}\right)^2}, \tag{5}$$

with η the viscosity of the saturating fluid and Λ' the thermal characteristic length. The "thermal resistivity" is related to the thermal characteristic length[27] through $R_t' = 8\tau_\infty\eta/\phi\Lambda'^2$. The thermal losses are usually neglected in water because the thermal diffusivity is ten times lower than the kinematic viscosity. Here, we nevertheless account for them and fix $\Lambda' = 2\Lambda$, where Λ is the viscous characteristic length. Thermal losses were considered relevant for modeling ultrasonic response of bones by some authors.[28,29]

In the absence of body forces, the conservation of momentum and the generalized Darcy's law lead to the following equations:

$$\begin{cases} \omega^2\rho_f\mathbf{w} + \omega^2\rho\mathbf{u} = -\nabla\cdot\boldsymbol{\sigma}, \\ \omega^2\rho_f\mathbf{u} + \omega^2\tilde{\rho}_{eq}\mathbf{w} = \nabla p, \end{cases} \tag{6}$$

where ρ is the bulk density of the porous medium, such that $\rho = (1-\phi)\rho_s + \phi\rho_f$, in which ρ_s is the density of the solid frame, and $\tilde{\rho}_{eq}$ is a mass parameter[3,30]

$$\tilde{\rho}_{eq} = \frac{\rho_f\tau_\infty}{\phi}\left(1 + \mathrm{i}\frac{\omega_c}{\omega}F(\omega)\right), \tag{7}$$

where $\omega_c = R_f\phi/\rho_f\tau_\infty$ is the Biot frequency with R_f the flow resistivity. The correction function $F(\omega)$ (Ref. 30) is given by

$$F(\omega) = \sqrt{1 - \mathrm{i}\eta\rho_f\omega\left(\frac{2\tau_\infty}{R_f\phi\Lambda}\right)^2}. \tag{8}$$

The mass parameter $\tilde{\rho}_{eq}$ is the complex frequency dependent equivalent density used in the rigid frame approximation, while the complex frequency dependent equivalent bulk modulus $\tilde{K}_{eq}$ used in this approximation is related to $\tilde{K}_f$ through $\tilde{K}_f = \phi\tilde{K}_{eq}$.

In the previous equations, μ, E_b, E_s, ν_b, ν_s, λ_c, α, M, ϕ, τ_∞, Λ', Λ, R_t', R_f are $\mathbf{x}$ dependent.

III. NUMERICAL EVALUATION OF THE SCATTERED PRESSURE FIELD

A. Description of the configuration

Both the incident plane acoustic wave and the tube are assumed to be invariant with respect to the x_3-coordinate, i.e., the tube axis. A cross-sectional $x_1 - x_2$ plane view of the 2D scattering problem is shown in Fig. 1.

The external and internal circular boundaries of the tube, whose radial coordinates are r^{ext} and r^{int}, are designated by Γ_{ext} and Γ_{int}. The porous material $M^{[1]}$ occupies the domain $\Omega^{[1]}$. The inhomogeneity occurs along the r direction, i.e., μ, E_b, E_s, ν_b, ν_s, λ_c, α, M, ϕ, τ_∞, Λ', Λ, R_t', R_f are r dependent. Isotropic macroscopically inhomogeneous porous materials

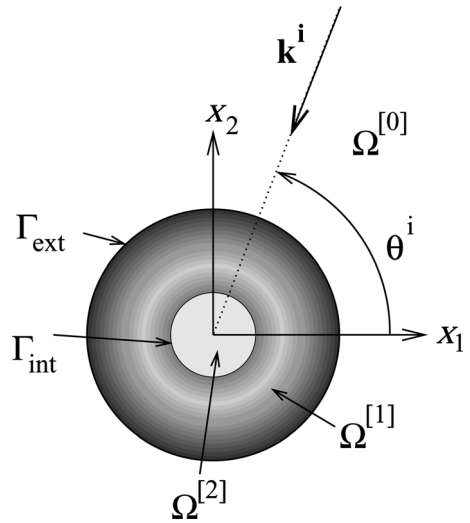

FIG. 1. Cross-sectional plane view of the configuration.

are considered. The material can be viewed either as functionally graded material or as a multilayer when the properties are piecewise constants. The ambient and saturating fluid is water [the density $\rho_f = 998\,\mathrm{kg\,m^{-3}}$, the bulk modulus $K_f = (1480)^2 \times \rho_f\,\mathrm{Pa}$, the viscosity $\eta = (1.0\times10^{-6})\times\rho_f\,\mathrm{kg\,m^{-1}\,s^{-1}}$, and Prandtl number $\mathrm{Pr} = 6,6$].

We denote the total pressure, wavenumber, and wave speed by the generic symbols p, k, and c, respectively, with $p = p^{[j]}$, $k = k^{[j]} = \omega/c^{[j]}$ in $\Omega^{[j]}$, $j = 0, 2$.

The wavevector $\mathbf{k}^i$ of the incident plane wave lies in the sagittal plane and the angle of incidence is θ^i measured counterclockwise from the positive x_1 axis. The incident wave propagates in $\Omega^{[0]}$ and is expressed by $p^i(\mathbf{x}) = A^i\sum_{n\in\mathbb{Z}}(-\mathrm{i})^n \mathrm{J}_n(k^{[0]}r)e^{in(\theta-\theta^i)}$, wherein J_n is the nth order Bessel function and $A^i = A^i(\omega)$ is the signal spectrum.

The uniqueness of the solution to the forward-scattering problem is ensured by the radiation condition

$$p^{[0]}(x) - p^i(\mathbf{x}) \sim e^{\mathrm{i}k^{[0]}\cdot\mathbf{x}}/\sqrt{|\mathbf{x}|}, \quad |\mathbf{x}| \to \infty. \tag{9}$$

B. The state vector formalism

We first introduce the Hankel like transform $\hat{s}(r,n)$ of $s(\mathbf{x})$. The latter can be simply written in the form $s(\mathbf{x}) = \sum_{n\in\mathbb{Z}}\hat{s}(r,n)e^{in\theta}$. The geometry of the configuration being circular, the fields components that are continuous along the inhomogeneity and the boundary conditions apply either to $s(\mathbf{x})$ or to $\hat{s}(r,n)$.

Inside the domain $\Omega^{[1]}$, the normal components of the total stress tensor $\sigma_{rr}^{[1]}$ and $\sigma_{r\theta}^{[1]}$, the pressure $p^{[1]}$, the solid displacement $u_r^{[1]}$ and $u_\theta^{[1]}$, and the normal component of the solid/fluid relative displacement $w_r^{[1]}$ are continuous fields. It could seem natural to choose these six parameters as components of the state vector. Nevertheless, in order to simplify algebraic manipulations it seems better to adapt these components to the considered boundary problem. At both interfaces Γ_{ext} and Γ_{int}, the stress tensor ($\sigma_{r\theta}^{[1]} = 0$, $\sigma_{rr}^{[1]} = -p^{[j]}$, $j = 0, 2$), the pressure ($p^{[1]} = p^{[j]}$, $j = 0, 2$), and normal component of the velocity $[-\mathrm{i}\omega(w_r^{[1]} + u_r^{[1]}) = V_r^{[j]}$, with $V_r^{[j]}$ the

radial component of the velocity in $\Omega^{[j]}$, $j=0,2]$, are continuous. Because $u_r^{[1]}$ and $w_r^{[1]}$ are continuous at any r in $\Omega^{[1]}$, $-\mathrm{i}\omega(w_r^{[1]}+u_r^{[1]})$ is also continuous. The radial component of the solid/fluid relative displacement $w_r^{[1]}$ is also replaced by $V_r^{[1]}=-\mathrm{i}\omega(w_r^{[1]}+u_r^{[1]})$ in Eqs. (1) and (6). This parameter is preferred to $w_r^{[1]}$ to define the wave vector. Moreover, after Hankel like transform of Eqs. (1) and (6), $r\widehat{\sigma}_{rr}^{[1]}=\widehat{\tau}_{rr}^{[1]}$ and $r\widehat{\sigma}_{r\theta}^{[1]}=\widehat{\tau}_{r\theta}^{[1]}$, appear more suitable than $\widehat{\sigma}_{rr}^{[1]}$ and $\widehat{\sigma}_{r\theta}^{[1]}$ to correctly cast the equations that have to be solved.

After this transform, these equations split into two systems of equations: one set of six first order differential equations only depending on the components of the column state vector $\widehat{\mathbf{W}}(r,n)=\langle\widehat{\tau_{rr}}^{[1]}(r,n),\widehat{\tau}_{r\theta}^{[1]}(r,n),\widehat{p}^{[1]}(r,n),\widehat{u}_r^{[1]}(r,n),\widehat{u}_\theta^{[1]}(r,n),\widehat{V}_r^{[1]}(r,n)\rangle$, and one set of two equations that linked the two last unknowns $\widehat{\tau}_{\theta\theta}^{[1]}(r,n)$ or, alternatively, $\widehat{\sigma}_{\theta\theta}^{[1]}(r,n)$ and $\widehat{w}_\theta^{[1]}(r,n)$, to the components of the state vector. The problem also reduces to the solution of the first order differential matrix system composed of the first six first order differential equations:

$$\frac{\partial}{\partial r}\widehat{\mathbf{W}}(r,n)-A(r,n)\widehat{\mathbf{W}}(r,n)=\mathbf{0}, \tag{10}$$

with $\mathbf{A}(r,n)=-\mathbf{B}(r,n)^{-1}\mathbf{D}(r,n)/r$, where

$$\mathbf{B}=\begin{bmatrix}1&0&0&-\lambda_c+\alpha M&0&-\frac{\mathrm{i}\alpha M}{\omega}\\0&1&0&\mathrm{i}n(\lambda_c-\alpha M)&0&\frac{-n\alpha M}{\omega}\\0&0&1&0&0&0\\0&0&0&M(\alpha-1)&0&\frac{\mathrm{i}M}{\omega}\\0&0&0&\lambda_c+2\mu-\alpha M&0&\frac{\mathrm{i}\alpha M}{\omega}\\0&0&0&0&\mu&0\end{bmatrix} \tag{11}$$

and

$$D=\begin{bmatrix}0&\mathrm{i}n&\frac{n^2\alpha M}{\tilde{\rho}_{eq}\omega^2 r}&-2\mu-\lambda_c+\alpha M+\omega^2r^2(\rho-\rho_f)&\mathrm{i}n\left(-2\mu-\lambda_c+\frac{\alpha M\rho_f}{\tilde{\rho}_{eq}}\right)&\frac{\mathrm{i}}{\omega}(\rho_f\omega^2r^2-\alpha M)\\0&1&\frac{\mathrm{i}n}{\tilde{\rho}_{eq}}\left(\rho_f r-\frac{n^2\alpha M}{\omega^2 r}\right)&\mathrm{i}n(2\mu+\lambda_c-\alpha M)&n^2\left(-2\mu-\lambda_c+\frac{\rho_f}{\tilde{\rho}_{eq}}\alpha M\right)+\omega^2r^2\left(\rho-\frac{\rho_f^2}{\tilde{\rho}_{eq}}\right)&\frac{-n\alpha M}{\omega}\\0&0&0&(\tilde{\rho}_{eq}-\rho_f)\omega^2r&0&-\mathrm{i}\tilde{\rho}_{eq}\omega r\\0&0&r-\frac{n^2M}{\tilde{\rho}_{eq}\omega^2r}&M(\alpha-1)&\mathrm{i}nM\left(\alpha-\frac{\rho_f}{\tilde{\rho}_{eq}}\right)&\frac{\mathrm{i}M}{\omega}\\-1&0&\frac{-n^2\alpha M}{\tilde{\rho}_{eq}\omega^2r}&\lambda_c-\alpha M&\mathrm{i}n\left(\lambda_c-\frac{\alpha M\rho_f}{\tilde{\rho}_{eq}}\right)&\frac{\mathrm{i}\alpha M}{\omega}\\0&-1&0&\mathrm{i}n\mu&-\mu&0\end{bmatrix}. \tag{12}$$

In practice, the matrix $\mathbf{B}$ is composed of the coefficients that appear in front of the first order dirivative of the components of $\widehat{\mathbf{W}}(r,n)$, while the matrix $\mathbf{D}$ is composed of the coefficients that appear in front of the components of $\widehat{\mathbf{W}}(r,n)$ in the first set of first order differential equations.

The matrices $\mathbf{B}$ and $\mathbf{D}$ are r-dependent, because $\lambda_c(r)$, $\alpha(r)$, $M(r)$, $\mu(r)$, $\tilde{\rho}_{eq}(r)$, and $\rho(r)$ are r-dependent. This dependence is not written in Eqs. (11) and (12) for conciseness. The expression of the matrix $\mathbf{A}$ clearly exhibits the intrinsic singularity on the cylinder axis. Here, tubes are considered, i.e., $r^{int}>0$, which greatly simplifies the solution of the mathematical problem. In the case of full inhomogeneous circular cylinder, a method like the one proposed in Ref. 12 can be used and adapted to deal with this singularity.

The solution of system (10) takes the form

$$\widehat{\mathbf{W}}(r^{ext},n)=\mathbf{M}(n)\widehat{\mathbf{W}}(r^{int},n), \tag{13}$$

where $\mathbf{M}$ is the so-called matricant,[20] which relates the value of the state vector $\widehat{\mathbf{W}}(r^{int},n)$, at $r=r^{int}$, to the value of the state vector $\widehat{\mathbf{W}}(r^{ext},n)$, at $r=r^{ext}$. Since $\mathbf{A}$ is r dependent, i.e., the tube is not homogeneous or piecewise constant, and $\mathbf{A}$ does not commute for different values of r, i.e., $[\mathbf{A}(r),\mathbf{A}(r')]=\mathbf{A}(r)\mathbf{A}(r')-\mathbf{A}(r')\mathbf{A}(r)\neq 0$, $\forall(r,r')\in[r^{int},r^{ext}]^2$, $r\neq r'$, the matricant $\mathbf{M}$ does not contain matrix exponentials or multiplications of matrix exponentials. The matricant is rather defined by the so-called multiplicative integral satisfying the Peano expansion.[19,20,31] This avoids any problem related to lack of discretization when the continuously varying material is approximated by a piecewise constant material. The Peano series reads as

$$\mathbf{M}(n)=\mathbf{I}+\int_{r^{int}}^{r^{ext}}\mathbf{A}(r,n)\mathrm{d}r+\int_{r^{int}}^{r^{ext}}\mathbf{A}(r,n)\left(\int_{r^{int}}^{r}\mathbf{A}(\zeta,n)\mathrm{d}\zeta\right)\mathrm{d}r+\cdots \tag{14}$$

and the evaluation of $\mathbf{M}(n)$ is performed via the iterative scheme

$$\begin{cases}\mathbf{M}(n)^{\{0\}}=\mathbf{I},\\ \mathbf{M}(n)^{\{m\}}=\mathbf{I}+\int_{r^{int}}^{r^{ext}}\mathbf{A}(r,n)\mathbf{M}(r,n)^{\{m-1\}}\mathrm{d}r,\end{cases} \tag{15}$$

such that

$$\lim_{m\to\infty} \mathbf{M}(n)^{\{m\}} = \mathbf{M}(n).$$

C. The boundary problem

The application of the boundary conditions at both interfaces Γ_{int} and Γ_{ext} [$\widehat{\tau}_{r\theta}^{[1]} = 0$, $\widehat{\tau}_{rr}^{[1]} = -r\widehat{p}^{[t]}$, $\widehat{p}^{[1]} = \widehat{p}^{[t]}$, and $\widehat{V}_r^{[1]} = \widehat{V}_r^{[t]} = -\mathrm{i}/\omega\rho(\partial\widehat{p}^{[t]}/\partial r)$, with $t = 0, 2$] yields the state vectors $\widehat{\mathbf{W}}(r^{ext}, n)$ and $\widehat{\mathbf{W}}(r^{int}, n)$, which are required to solve the problem. Separation of variables, the radiation conditions, and Hankel-like transform lead to the representations

$$\begin{aligned}\widehat{p}^{[0]}(r,n) &= \mathrm{J}_n(k^{[0]}r)(-\mathrm{i})^n e^{-\mathrm{i}n\theta^i} + R_n \mathrm{H}_n^{(1)}(k^{[0]}r),\\ \widehat{p}^{[2]}(r,n) &= T_n \mathrm{J}_n(k^{[2]}r).\end{aligned} \tag{16}$$

The application of the boundary conditions at the interface Γ_{ext} and Γ_{int} leads to

$$\begin{aligned}\widehat{\mathbf{W}}(n, r^{ext}) &= \mathbf{L}^{ext}(n)\begin{bmatrix} R_n \\ \widehat{u}_r^{[1]}(r^{ext}, n) \\ \widehat{u}_\theta^{[1]}(r^{ext}, n)\end{bmatrix} + \mathbf{S}(n) \quad \text{and}\\ \widehat{\mathbf{W}}(n, r^{int}) &= \mathbf{L}^{int}(n)\begin{bmatrix} T_n \\ \widehat{u}_r^{[1]}(r^{int}, n) \\ \widehat{u}_\theta^{[1]}(r^{int}, n)\end{bmatrix},\end{aligned} \tag{17}$$

with

$$\mathbf{L}^{ext}(n) = \begin{bmatrix} -r^{ext}\mathrm{H}_n^{(1)}(k^{[0]}r^{ext}) & 0 & 0 \\ 0 & 0 & 0 \\ \mathrm{H}_n^{(1)}(k^{[0]}r^{ext}) & 0 & 0 \\ 0 & 1 & 0 \\ 0 & 0 & 1 \\ \dfrac{-\mathrm{i}k^{[0]}\dot{H}_n^{(1)}(k^{[0]}r^{ext})}{\omega\rho^{[0]}} & 0 & 0 \end{bmatrix},$$

$$\mathbf{L}^{int}(n) = \begin{bmatrix} -r^{int}\mathrm{J}_n(k^{[2]}r^{int}) & 0 & 0 \\ 0 & 0 & 0 \\ \mathrm{J}_n(k^{[2]}r^{int}) & 0 & 0 \\ 0 & 1 & 0 \\ 0 & 0 & 1 \\ \dfrac{-\mathrm{i}k^{[2]}\dot{J}_n(k^{[2]}r^{int})}{\omega\rho^{[2]}} & 0 & 0 \end{bmatrix}, \tag{18}$$

where $\dot{\chi} = \partial\chi/\partial r$, $\chi = \mathrm{J}_n$, or $\chi = \mathrm{H}_n^{(1)}$, and

$$\mathbf{S}(n) = \begin{bmatrix} -r^{ext}\mathrm{J}_n(k^{[0]}r^{ext})(-\mathrm{i})^n e^{-\mathrm{i}n\theta^i} \\ 0 \\ \mathrm{J}_n(k^{[0]}r^{ext})(-\mathrm{i})^n e^{-\mathrm{i}n\theta^i} \\ 0 \\ 0 \\ \dfrac{-\mathrm{i}k^{[0]}\dot{\mathrm{J}}_n(k^{[0]}r^{ext})(-\mathrm{i})^n e^{-\mathrm{i}n\theta^i}}{\omega\rho^{[0]}} \end{bmatrix}. \tag{19}$$

The excitation of the system by the incident plane wave is accounted for in $\mathbf{S}$, $\mathbf{L}^{ext}$ relates the unknowns R_n, $\widehat{u}_r^{[1]}(r^{ext}, n)$ and $\widehat{u}_\theta^{[1]}(r^{ext}, n)$ to the state vector $\widehat{\mathbf{W}}(r^{ext}, n)$, and $\mathbf{L}^{int}$ relates the unknowns T_n, $\widehat{u}_r^{[1]}(r^{int}, n)$ and $\widehat{u}_\theta^{[1]}(r^{int}, n)$ to the state vector $\widehat{\mathbf{W}}(r^{int}, n)$.

Finally, introducing Eq. (17) in (13), the final system of equations for the solution in terms of R_n and T_n can be cast in the form

$$[[\mathbf{L}^{ext}][-\mathbf{M}\mathbf{L}^{int}]]\begin{bmatrix} R_n \\ \widehat{u}_r^{[1]}(r^{ext}, n) \\ \widehat{u}_\theta^{[1]}(r^{ext}, n) \\ T_n \\ \widehat{u}_r^{[1]}(r^{int}, n) \\ \widehat{u}_\theta^{[1]}(r^{int}, n)\end{bmatrix} = -\mathbf{S}(n).$$

This system is solved for each frequency and each order n and directly provides the reflection and transmission coefficients associated with the incident wave of indice n. The pressure fields in $\Omega^{[0]}$ and $\Omega^{[2]}$ can be calculated through

$$\begin{aligned}p^{[0]}(\mathbf{x}) &= A^i \sum_{n\in\mathbb{Z}} [\mathrm{J}_n(k^{[0]}r)(-\mathrm{i})^n e^{-\mathrm{i}n\theta^i} + R_n \mathrm{H}_n^{(1)}(k^{[0]}r)]\ e^{\mathrm{i}n\theta},\\ p^{[2]}(\mathbf{x}) &= A^i \sum_{n\in\mathbb{Z}} T_n \mathrm{J}_n(k^{[0]}r) e^{\mathrm{i}n\theta}.\end{aligned} \tag{20}$$

The pressure field in $\Omega^{[0]}$ can be split into the incident and the scattered fields.

IV. VALIDATION ON A MULTILAYERED POROUS MEDIUM

In order to validate the present method, calculations are performed for a known two-layer poroelastic medium configuration considered as a single poroelastic tube. Each layer of the tube is a porous material saturated by water. Materials $M^{[0]}$ and $M^{[2]}$ are also water. The characteristic properties of each layer have been given in Refs. 16 and 17 and are recalled in Table I. The layer L2 is supposed to model cancellous bone, while layer L1 is supposed to model cortial bone. The geometrical parameters are close to those of a human femur. The values of cancellous bone are those recovered in Ref. 17, while those of the cortical bone have been chosen in accordance with those of the solid frame. Effectively, cortical bone has mainly been modeled, for instance, as an elastic material,[32,33] because it has a porosity around 0.1. Therefore, only a few poroelastic parameters of cortical bone are available in the literature. The solid frame is bone elastic material. The Young modulus E_s and Poisson ratio ν_s are also identical for both cortical and cancellous bone. The Young's modulus and Poisson's ratio of the skeleton, which can be seen as the apparent solid part of the porous material itself, are also closer to E_s and ν_s, because osteons are packed tightly in cortical bones. Both characteristic lengths are geometrical parameters of the pore-size distribution inside the porous sample. The thermal characteristic length represents a measure of the average pore size, while the viscous characteristic length corresponds to the average size of the "constrictions" in the porous medium, i.e., the average distance between pore walls in the

TABLE I. Properties of the two-layer medium studied.

	ϕ	τ_∞	Λ (μm)	Λ' (μm)	R_f (N s m^{-4})
L2	0.64	1	10	20	10 000
L1	0.1	1	1	2	100 000

	ρ_s (kg m^{-3})	E_b (Pa)	ν_b	E_s (Pa)	ν_s	Th (mm)
L2	1990	4.49×10^9	0.28	1.3×10^{10}	0.3	5
L1	1990	1.29×10^{10}	0.29	1.3×10^{10}	0.3	5

narrower areas of the pore volume. Both characteristic lengths are smaller in cortical bones than in cancellous bones. Moreover, the flow resistivity, which is related to the porosity, should be much higher in cortical than in cancellous bone. The tortuosity is kept at unity. The elastic damping d is accounted for through complex shear moduli and therefore complex Young moduli of both the solid frame and skeleton. The shear moduli are evaluated through $\mu = E(1 - id)/2(1+\nu)$ from the knowledge of E and ν. This elastic damping is fixed at $d = 0.05$ for both the solid frame and skeleton.

The choice of this configuration is motivated by the fact that the results of the present method can be compared with known results from the classical transfer matrix method (TMM), or domain separation, based on the initial formulation of Biot 1956,[25] which can be easily derived from various publications,[9] and is briefly summarized in the Appendix.

To consider the bilayer tube as a single inhomogeneous tube, the jump discontinuity in the two-layered system is smoothed by using the following analytical continuous and continuously differentiable function

$$I(r) = 1 + \frac{C}{2}\left[1 + \mathrm{erf}\left(\frac{r - r^j}{s}\right)\right], \tag{21}$$

where C is the step value, which is different for each parameter in Table I, erf is the error function, r^j is the position of the jump, and s corresponds to the steepness of the continuous jump such that the smaller s is, the steeper the jump is.

The number of iterations required for the correct evaluation of the matricant increases with frequency. A change of variable like the one proposed in Refs. 34 and 35 seems inaccurate, because the characteristic parameters are frequency dependent for porous materials. Moreover, a large number of iterations is required for the correct evaluation, because poroelastic materials are highly dissipative.

The configuration is discretized with 3000 points and the number of iterations for the evaluation of the Peano series is 300. These values were not optimized, but it was found that the spatial discretization along the inhomogeneity should be small compared to the wavelength inside the porous material for the method to correctly model the response. The jump position and its slope are fixed to $r^j = (r^{ext} - r^{int})/2 = 10\,\mathrm{mm}$ and $s = 10^{-6}$, while $r^{int} = 5\,\mathrm{mm}$ and $r^{ext} = 15\,\mathrm{mm}$. The infinite sum $\sum_{m\in\mathbb{Z}}$ over the indices of the modal representation of the diffracted field by a cylinder is truncated[36] as $\Sigma_{m=-M}^{M}$ such that $M = \mathrm{int}(\mathrm{Re}(4.05 \times (k^{[1]}R)^{1/3} + k^{[1]}R)) + 10$.

Figure 2 depicts a comparison between the pressure field scattered by the inhomogeneous poroelastic tube, supposed to model an appendicular human bone, calculated with the classical TMM and the present method at $\theta^{mes} = \theta^i$ and $r^{mes} = 50\,\mathrm{mm}$. Both curves coincide.

V. NUMERICAL EXAMPLE ON DIFFERENT INHOMOGENEITY PROFILES

Osteoporosis is characterized by a decrease of the cortical bone thickness and an increase of the porosity of the cancellous bone. As an example of variation of the parameters, the profile of flow resistivity R_f is plotted on the same figure as the time domain response of the corresponding configuration in Fig. 3. The other parameters vary with an identical profile. Figure 3(a) depicts the time domain scattered field by the previous two-layer configuration, when a Ricker like pulse centered at $\nu_0 = 50\,\mathrm{kHz}$ impinges the tube (at $\theta^i = 0$), at 90 measurement points around the tube running from $\theta^{mes} - \theta^i = 0$ to $\theta^{mes} - \theta^i = 2\pi$ for a fixed radius $r^{mes} = 50\,\mathrm{mm}$. The Ricker-like pulse spectrum is given by

$$A^i = \frac{\omega^2}{4\sqrt{\pi}(\pi\nu_0)^3} e^{\mathrm{i}(\omega/\nu_0) - \omega^2/(2\pi\nu_0)^2}. \tag{22}$$

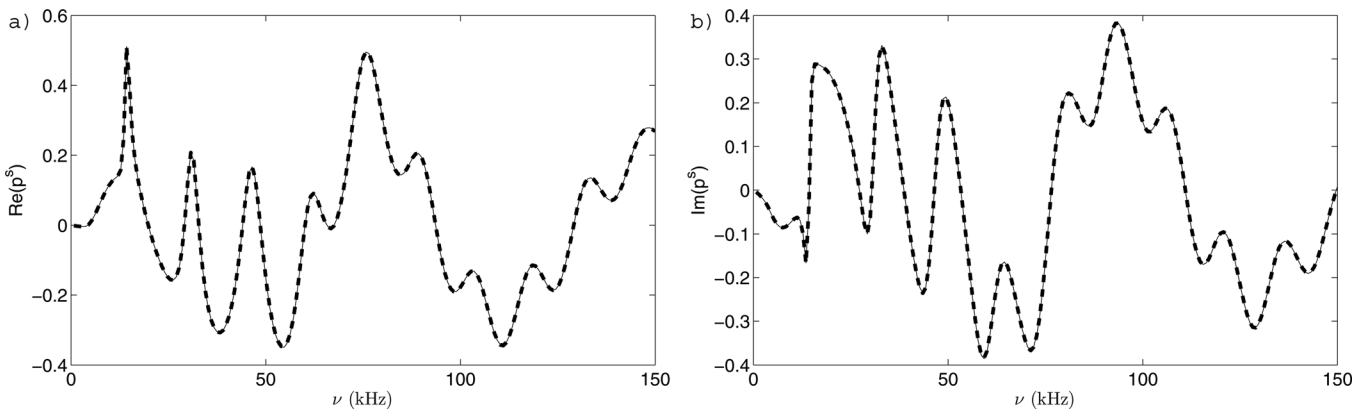

FIG. 2. Real (a) and imaginary (b) parts of the scattered pressure field by the two-layered tube calculated with the classical TMM (—) and with the present method (– – –) at $\theta^{mes} = \theta^i$ and $r^{mes} = 50\,\mathrm{mm}$.

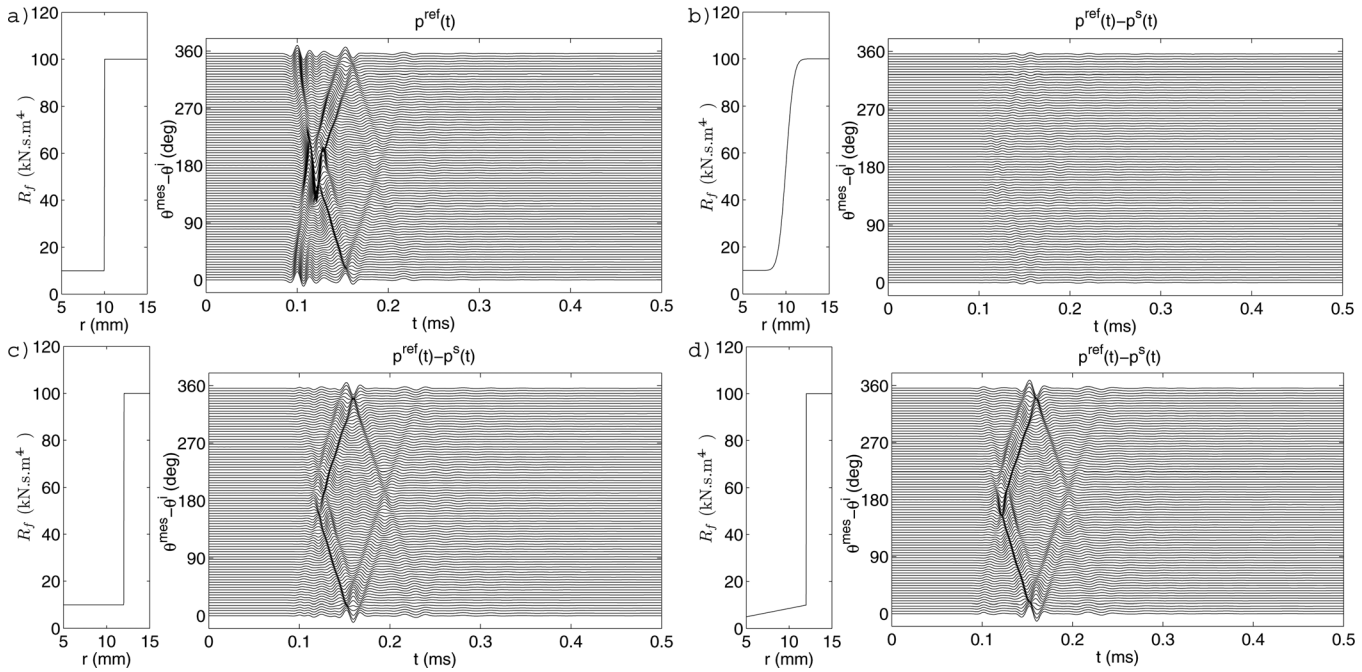

FIG. 3. Time domain scattered fields by the reference configuration (a), and differences of the time domain scattered fields by the reference configuration and by configurations with various inhomogeneity profiles (b), (c), and (d). The profile of the flow resistivity R_f is plotted as an example of variation of the parameters.

Most of the previous studies, mainly based on axial transmission,[14,15] employed excitations between 500 kHz to 3 MHz. In order for the wave to strongly and deeply interact with the bone structure, the frequency of the chosen excitation stands in the low frequency ultrasonic regime at $\nu_0 = 50$ kHz. Moreover a low frequency ultrasonic excitation renders the hypothesis of a circular cross-section more valid, because a long bone is obviously not of perfectly circular cross-section. The scattered field $p^{ref}(t)$ is also symmetric with respect to $\theta^{mes} - \theta^i = \pi$. This configuration is then considered as the reference configuration.

Most of the methods that are used to solve inverse problems of material characterization are based on the comparison of the response of a reference configuration with the response of the configuration that has to be characterized. The comparison of these responses can then be interpreted by use of an integral formulation involving the specific dyadic Green's function of the configuration. The closer the reference configuration is to the to-be-characterized configuration, the easier is the solution of the inverse problem. Nevertheless, the amplitude of the differences has to be sufficiently large to be measured, i.e., to overcome signal to noise problems, and interpreted. Figures 3(b), 3(c), and 3(d) depict the differences of the time domain scattered fields by the reference configuration $p^{ref}(t)$ and by various configurations $p^s(t)$ that could be encountered in case of bone degradation due to osteoporosis. The amplitude scale of the four subfigures of Fig. 3 are identical.

Figure 3(b) depicts the difference between the time domain scattered field by the reference configuration ($s = 10^{-6}$) and a smoother jump from the value of L1 to L2 configuration, with $s = 10^{-3}$. The differences are not particularly noticeable. The amplitude of $p^{ref}(t) - p^s(t)$ is in this case relatively small. A smoother jump could be difficult to be determined or interpreted.

Figure 3(c) depicts the difference between the time domain scattered field by the reference configuration (with $r^j = 10$ mm) and by a thinner cortical bone configuration (with $r^j = 12$ mm). The amplitude of $p^{ref}(t) - p^s(t)$ is this time of the same order of magnitude as the scattered field by the reference configuration. This means that the scattered ultrasonic field is sensitive to the cortical thickness.

To go further on, the properties are supposed to vary linearly between r^{int} and $r^j = 12$ mm from the value of L_{in} Table II to those of Table I at r^j. The porosity of the inner poroelastic material is larger. The solid frame is the bone elastic material. The Young modulus E_s and Poisson ratio ν_s are also identical. The Young's modulus and Poisson's ratio of the skeleton are smaller than E_b and ν_b of L2. Both characteristic lengths are also larger in L_{in} than in L2. It should be noted that some bones exhibit visible heterogeneity, which would indicate higher values for these lengths. Moreover, the flow resistivity, which is related to the porosity, should be smaller in L_{in} than L2. The tortuosity is kept around unity. Figure 3(d) depicts the difference of the time domain response of the reference configuration with the thinner cortical bone and a linear variation of the parameters along the cancellous bone thickness. The amplitude of $p^{ref}(t) - p^s(t)$ is once again of the same order of magnitude as the scattered field by the reference configuration. This

TABLE II. Properties of the inner part of the tube.

	ϕ	τ_∞	Λ (μm)	Λ' (μm)	R_f (N s m^{-4})
L_{in}	0.8	1.1	30	60	5000
	ρ_s (kg m^{-3})	E_b (Pa)	ν_b	E_s (Pa)	ν_s
L_{in}	1990	2.49×10^9	0.28	1.3×10^{10}	0.3

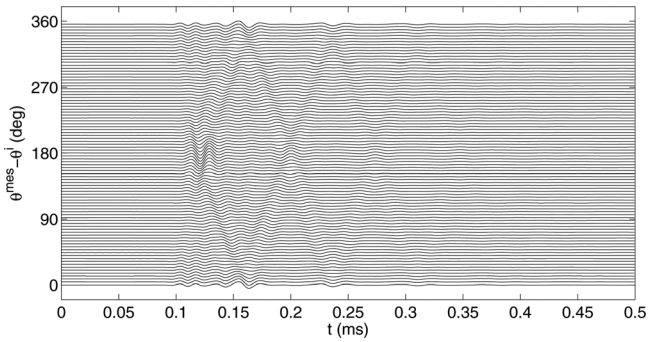

FIG. 4. Difference between the time domain response scattered pressure field by the thinner cortical bone configuration ($r^j = 12\,\text{mm}$) and a thinner cortical bone with a linear variation of the parameters calculated with the present method at $r^{mes} = 50\,\text{mm}$ for $\theta^{mes} \in [0; 2\pi]$.

means that the scattered ultrasonic field is sensitive to the cortical thickness and cancellous bone parameter variations. To emphasize the sensitivity to the parameter variation of the cancellous bone, Fig. 4 depicts the difference of the time domain response of the thinner cortical bone configuration ($r^j = 12\,\text{mm}$) with the previous configuration, i.e., with the one of the linear variation of the spongy bone parameters. The scattered field is also sensitive to the variation of the cancellous bone parameters.

VI. CONCLUSION

A model of the acoustic response of macroscopically inhomogeneous elastic frame porous materials derived from the alternative Biot's theory of 1962 was solved. A stable numerical method, derived from the state vector formalism together with Peano series was developed to solve the macroscopically inhomogeneous poroelastic wave equations. To our knowledge, these equations are solved and these methods are derived for the first time for poroelastic materials in a cylindrical configuration. A validation of this method was made using the example of a two-layer tube supposed to model a long bone excited in the sagittal plane, by comparison to the exact solution obtained by the transfer matrix method. In the numerical procedure, the jump of properties between the layers was accounted for in the form of a single continuous function. This result validates the present procedure. Finally, examples of the time domain response are given for various property profiles. These examples illustrate the possibility of modeling long bones as macroscopically inhomogeneous poroelastic tubes, which can be therefore used for the osteoporosis diagnose. This last point requires further investigation, notably the development of a three-dimensional macroscopically inhomogeneous poroelastic tube model that accounts for the anisotropy of the cortical bone. Another important improvement yields in the accounting for marrow parameters and particularly for the marrow viscosity. This could be accounted for in our calculation by considering various saturating fluids, without loss of generality of the method. As pointed out in the Introduction, other applications, mainly related to varying property poroelastic materials offering better sound absorption than homogeneous ones can be investigated by use of the described method.

ACKNOWLEDGMENT

The authors would like to thank Armand Wirgin for discussions and his useful help during the writing of the paper.

APPENDIX: TRANSFER MATRIX METHOD FOR THE TWO-LAYER TUBE

Separation of variables and the radiation condition leads to the representations in Eq. (20) of $\Omega^{[0]}$ and $\Omega^{[2]}$. The initial Biot formulation[25] is used to model the acoustic wave propagation in the two homogeneous layers. In both layers, the two scalar, $\phi_1^{[Li]}$ and $\phi_2^{[Li]}$, and vector, $\psi^{[Li]} = \psi^{[Li]}\mathbf{i}_3$, potentials related to the solid displacement $\mathbf{u}^{[Li]}$ through $\mathbf{u}^{[Li]} = \nabla\left(\phi_1^{[Li]} + \phi_2^{[Li]}\right) + \nabla \times \psi^{[Li]}$ and to the fluid displacement $\mathbf{U}^{[Li]} = \mathbf{\nabla}(\mu_1^{[Li]}\phi_1^{[Li]} + \mu_2^{[Li]}\phi_2^{[Li]}) + \nabla \times \mu_3^{[Li]}\psi^{[Li]}$ take the forms

$$\begin{aligned}
\phi_1^{[Li]} &= \sum_{n\in\mathbb{Z}} \left(C_n^{[Li]}\mathrm{H}_n^{(1)}(k_1^{[Li]}r) + D_n^{[Li]}\mathrm{J}_n(k_1^{[Li]}r)\right) e^{in\theta},\\
\phi_2^{[Li]} &= \sum_{n\in\mathbb{Z}} \left(E_n^{[Li]}\mathrm{H}_n^{(1)}(k_2^{[Li]}r) + F_n^{[Li]}\mathrm{J}_n(k_2^{[Li]}r)\right) e^{in\theta},\\
\psi^{[Li]} &= \sum_{n\in\mathbb{Z}} \left(G_n^{[Li]}\mathrm{H}_n^{(1)}(k_3^{[Li]}r) + I_n^{[Li]}\mathrm{J}_n(k_3^{[Li]}r)\right) e^{in\theta}, \qquad \text{(A1)}
\end{aligned}$$

$i = 1, 2$. In these potential expressions, $k_j^{[Li]}$, $i = 1, 2$, $j = 1, 2, 3$, are the wave numbers respectively associated with the so-called fast, slow and shear waves. The expressions of $k_j^{[Li]}$ as well as those of the amplitude ratio (the so-called compatibility coefficients) $\mu_j^{[Li]}$, $i = 1, 2$, $j = 1, 2, 3$, can be found in Ref. 26. The unknows $C_n^{[Li]}$, $E_n^{[Li]}$, and $G_n^{[Li]}$, are associated with the in-going waves, while the unknowns $D_n^{[Li]}$, $F_n^{[Li]}$, and $I_n^{[Li]}$, are associated with the out-going waves in layer Li, $i = 1, 2$. The constitutive relations in both layers read as

$$\begin{aligned}
\sigma_{ij}^{s[Lm]} &= \left[\left(P^{[Lm]} - 2N^{[Lm]}\right)\varepsilon_{ii}^{[Lm]} + Q^{[Lm]}e_{ii}^{[Lm]}\right]\delta_{ij} \\
&\quad + 2N^{[Lm]}\varepsilon_{ij}^{[Lm]} \\
&= \left[a_1^{[Lm]}\left(k_1^{[Lm]}\right)^2\phi_1^{[Lm]} + a_2^{[Lm]}\left(k_2^{[Lm]}\right)^2\phi_2^{[Lm]}\right]\delta_{ij} \\
&\quad + 2N^{[Lm]}e_{ij}^{[Lm]}, \\
\sigma_{ij}^{f[Lm]} &= \left[Q^{[Lm]}\varepsilon_{ii}^{[Lm]} + R^{[Lm]}e_{ii}^{[Lm]}\right]\delta_{ij} = -\phi^{[Lm]}p^{[Lm]}\delta_{ij} \\
&= -\left[b_1^{[Lm]}\left(k_1^{[Lm]}\right)^2\phi_1^{[Lm]} + b_2^{[Lm]}\left(k_2^{[Lm]}\right)^2\phi_2^{[Lm]}\right]\delta_{ij}, \qquad \text{(A2)}
\end{aligned}$$

where the components of the stress tensor of the solid and fluid phases are $\sigma_{ij}^{s[Lm]}$ and $\sigma_{ij}^{f[Lm]}$, $a_i^{[Lm]} = 2N^{[Lm]} - P^{[Lm]} - Q^{[Lm]}\mu_i^{[Lm]}$, and $b_i^{[Lm]} = Q^{[Lm]} + R^{[Lm]}\mu_i^{[Lm]}$, $i = 1, 2$, and $e_{ij}^{[Lm]} = 1/2(U_{i,j}^{[Lm]} + U_{j,i}^{[Lm]})$, $m = 1, 2$. The expression of the coefficients P, Q, R are given in Eq. (3).

At the interfaces Γ_{ext} between $\Omega^{[0]}$ and the layer L1 and Γ_{int} between the layer L2 and $\Omega^{[2]}$, the total stress, pressure, and normal component of the displacement are continuous, i.e.,

$$\begin{aligned}
&\sigma_{rr}^{s[L1]} + \sigma_{rr}^{f[L1]} + p^{[0]} = 0, && \sigma_{rr}^{s[L2]} + \sigma_{rr}^{f[L2]} + p^{[2]} = 0,\\
&\sigma_{r\theta}^{s[L1]} = 0, && \sigma_{r\theta}^{s[L1]} = 0,\\
&\sigma_{rr}^{f[L1]}/\phi^{L1} + p^{[0]} = 0, && \sigma_{rr}^{f[L2]}/\phi^{L2} + p^{[2]} = 0,\\
&\phi^{L1}U_r^{[L1]} + (1-\phi^{L1})u_r^{[L1]} - U_r^{[0]} = 0, && \phi^{[L2]}U_r^{[L2]} + (1-\phi^{[L2]})u_r^{[L2]} - U_r^{[2]} = 0,
\end{aligned} \tag{A3}$$

where $U_r^{[i]} = (1/\rho^{[i]}\omega^2)(\partial p^{[i]}/\partial r)$, $i = 0, 2$. At the interface between the two layers L1 and L2, the total stress, pressure, solid displacement and normal component of the solid/fluid displacement are continuous, i.e.,

$$\begin{aligned}
&\sigma_{rr}^{s[L1]} + \sigma_{rr}^{f[L1]} - \sigma_{rr}^{s[L2]} - \sigma_{rr}^{f[L2]} = 0, && \sigma_{r\theta}^{s[L1]} - \sigma_{r\theta}^{s[L2]} = 0,\\
&\sigma_{rr}^{f[L1]}/\phi^{L1} - \sigma_{rr}^{f[L1]}/\phi^{L1} = 0, && u_r^{[L1]} - u_r^{[L2]} = 0,\\
&u_\theta^{[L1]} - u_\theta^{[L2]} = 0, && \phi^{[L1]}(U_r^{[L1]} + u_r^{[L1]}) - \phi^{[L2]}(U_r^{[L2]} + u_r^{[L2]}) = 0.
\end{aligned} \tag{A4}$$

Introducing the potential expressions Eq. (A1) in Eqs. (A3) and (A4) leads, after projection on $\int_0^{2\pi} e^{-il\theta}d\theta$ and making use of the orthogonality relation $\int_0^{2\pi} e^{i(n-l)\theta}d\theta = 2\pi\delta_{ln}$, to a 14×14 linear system of equations for the solution of the mathematical problem, in particular in terms of R_n and T_n. This system is solved for each frequency and for each n. Once solved, the scattered field by the two layer tube can be evaluated through Eq. (20).

[1]L. De Ryck, W. Lauriks, Z. Fellah, A. Wirgin, J. Groby, P. Leclaire, and C. Depollier, "Acoustic wave propagation and internal fields in rigid frame macroscopically inhomogeneous porous media," J. Appl. Phys. **102**, 024910 (2007).

[2]L. De Ryck, W. Lauriks, P. Leclaire, A. Wirgin, J. Groby, and C. Depollier, "Reconstruction of material properties profiles in one-dimensional macroscopically inhomogeneous rigid frame porous media in the frequency domain," J. Acoust. Soc. Am. **124**, 1591–1606 (2008).

[3]M. Biot, "Mechanics of deformation and acoustic propagation in porous media," J. Appl. Phys. **33**, 1482–1498 (1962).

[4]L. De Ryck, J.-P. Groby, P. Leclaire, W. Lauriks, A. Wirgin, C. Depollier, and Z. Fellah, "Acoustic wave propagation in a macroscopically inhomogeneous porous medium saturated by a fluid," Appl. Phys. Lett. **90**, 181901 (2007).

[5]J.-P. Groby, L. De Ryck, P. Leclaire, A. Wirgin, W. Lauriks, R. P. Gilbert, and Y. Xu, "Use of specific Green's functions for solving direct problems involving a heterogeneous rigid frame porous medium slab solicited by acoustic waves," Math. Meth. Appl. Sci. **30**, 91–122 (2007).

[6]G. Gautier, J. P. Groby, O. Dazel, L. Kelders, L. De Ryck, and P. Leclaire, "Propagation of acoustic waves in a one-dimensional macroscopically inhomogeneous poroelastic material," J. Acoust. Soc. Am. **130**, 1390–1398 (2011).

[7]O. Omnova, K. Attenborough, and C. Linton, "Effects of porous covering on sound attenuation by periodic arrays of cylinders," J. Acoust. Soc. Am. **119**, 278–284 (2006).

[8]C. Wisse, D. Smeulders, G. Chao, and M. van Dongen, "Guided waves modes in porous cylinders: Theory," J. Acoust. Soc. Am. **122**, 2049–2056 (2007).

[9]S. Hasheminedjad and R. Avzmohammdi, "Elastic wave scattering in porous unidirectional fiber-reinforced composites," J. Reinforced Palst. Comp. **26**, 495–517 (2007).

[10]A. Shuvalov, O. Poncelet, and M. Deschamps, "General formalism for plane guided waves in transversely inhomogeneous anisotropic plates," Wave Motion **40**, 413–426 (2004).

[11]A. Shuvalov, "A sectic formalism for three-dimansional elastodynamics of cylindrically anisotropic radially inhomogeneous materials," Proc. R. Soc. London, Ser. A **459**, 1611–1639 (2003).

[12]A. Norris and A. Shuvalov, "Wave impedance matrices for cylindrically anisotropic radially inhomogeneous elastic solids," arXiv:1003.5713v2.

[13]C. Baron, "Propagation of elastic waves in an anisotropic radially graded cylindrical waveguide: Application to bone evaluation," in *Proceedings of the 10th French Congress of Acoustics* (2010).

[14]E. Bossy, M. Talmant, and P. Laugier, "Three-dimensional simulations fo ultrasonic axial transmission velovity measurement on cortical bone models," J. Acoust. Soc. Am. **115**, 2314–2324 (2004).

[15]G. Haita, S. Saili, Q. Grimal, M. Talman, C. Desceliers, and C. Soize, "Influence of a gradient of material properties on ultrsonic wave propagation in cortical bone: Application to axial transmission," J. Acoust. Soc. Am. **125**, 4043–4052 (2009).

[16]A. Pakula, F. Padilla, P. Laugier, and M. Kaczmarek, "Application of Biot's theory to ultrasonic characterization of human cancellous bones: Determination of structural, material, and mechanical properties," J. Acoust. Soc. Am. **123**, 2415–2423 (2008).

[17]N. Sebaa, Z. Fellah, E. Ogam, A. Wirgin, F. Mitri, C. Depollier, and W. Lauriks, "Ultrasonic characterization of human cancellous bone using the biot theory: Inverse problem," J. Acoust. Soc. Am. **120**, 1816–1824 (2006).

[18]A. Stroh, "Steady state problems in anisotropic elasticity," J. Math. Phys. **41**, 77–103 (1962).

[19]G. Peano, "Intégration par série des équations différentielles linéaires (Integration of linear differential equation by series expansion)," Math. Ann. **32**, 450–456 (1888).

[20]M. Pease, *Methods of Matrix Algebra* (Academic Press, New York, 1965), Chaps. 6 and 7.

[21]M. Carcione, *Wavefield in Real Media: Wave Propagation in Anisotropic, Anelastic and Porous Media* (Pergamon, New York, 2001), Chap. 7.

[22]S. Pride and J. Berryman, "Connecting theory to experiment in poroelasticity," J. Mech. Phys. Solids **46**, 719–747 (1998).

[23]O. Dazel, B. Brouard, C. Depollier, and S. Griffiths, "An alternative biot's displacement formulation for porous materials," J. Acoust. Soc. Am. **121**, 3509–3516 (2007).

[24]M. Biot and D. Willis, "The elastic coefficients of the theory of consolidation," J. Appl. Mech. **24**, 594–601 (1957).

[25]M. Biot, "Theory of propagation of elastic waves in fluid-saturated porous solid," J. Acoust. Soc. Am. **28**, 168–178 (1956).

[26]J.-F. Allard and N. Atalla, *Propagation of Sound in Porous Media: Modelling Sound Absorbing Materials* (Wiley, Chichester, 2006), Chaps. 5 and 6.

[27]J.-F. Allard and Y. Champoux, "New empirical equations for sound propagation in rigid frame porous materials," J. Acoust. Soc. Am. **91**, 3346–3353 (1992).

[28]I. Kang, R. Heui-Seol, and W. Suk, "Acoustic wave propagation in bovine cancellous bone: Application of the modified Biot-Attenborough model," J. Acoust. Soc. Am. **114**, 2284–2293 (2003).

[29]I. Kang and W. Suk, "Comparison of acoustic characteristics predicted by Biot's theory and the the modified Biot-Attenborough model in cancellous bone," J. Biomech. **39**, 364–368 (2006).

[30]D. Johnson, J. Koplik, and R. Dashen, "Theory of dynamic permeability and tortuosity in fluid-saturated porous media," J. Fluid Mech. **176**, 379–402 (1987).

[31]C. Baron, "Le développement en série de peano du matricant pour l'étude de la propagation des ondes élastiques en milieux a proprités continuement variables (Matricant Peano series development to study elastic waves propagation in continuously varying properties materials)," Ph.D. thesis, Université de Bordeaux I (2005).
[32]X. Dong and X. Guo, "The dependence of transversely isotropic elasticity of human femoral cortical bone on porosity," J. Biomech. **37**, 1281–1287 (2004).
[33]A. Said, K. Raum, I. Leguerney, and P. Laugier, "Spatial distribution of anisotropic acoustic impedance assessed by time-resolved 50-Mhz scanning microscopy and its relation to porosity in human cortical bone," Bone **43**, 187–194 (2008).
[34]N. Haskell, "The dispersion of surface waves on multilayered media," Bull. Seism. Soc. Am. **43**, 377–393 (1953).
[35]W. Thomson, "Transmission of elastic wave through a stratified solid medium," J. Appl. Phys. **21**, 89–93 (1950).
[36]P. Barber and S. Hill, *Light Scattering by Particles: Computation Methods*, Vol. 2 of Advanced Series in Applied Physics (World Scientific, London, 1990), Chap. 2, p. 30.